Journal of Molecular Liquids 414 (2024) 126174

Contents lists available at ScienceDirect

Journal of Molecular Liquids

journal homepage: www.elsevier.com/locate/molliq

The influence of bromine substitution and linking groups on the phase behaviour of light-responsive rod-like molecules

Mohamed Alaasar [a,b,*], Tejal Nirgude [a], Christian Anders [a]

[a] Institute of Chemistry, Martin Luther University Halle-Wittenberg, 06120 Halle, Germany
[b] Department of Chemistry, Faculty of Science, Cairo University, 12613 Giza, Egypt

ARTICLE INFO

Keywords:
Liquid crystals
Nematic phase
Azobenzene
Bromination
Smectic phase
Cybotactic clusters

ABSTRACT

The effect of aromatic core bromination as well as different linking groups on the phase behaviour of light-responsive rod-like liquid crystalline materials is reported. For this purpose, two new series of laterally brominated rod-like molecules are designed and synthesized. The two series have three benzene rings connected using different linking groups either azo or ester units with different directions. Both series have pentyloxy chain at one end and an octyl chain at the other end in the first group or an octyloxy chain in the second group of materials. Additional lateral bromine substituent was inserted at ortho position with respect to the pentyloxy chain. The molecular self-assembly of the new materials was investigated using polarized optical microscope (POM), differential scanning calorimetry (DSC) and X-Ray diffraction (XRD). Depending on the type of the terminal chain (octyl or octyloxy) at one end and nature of the linking groups nematic phases as well as smectic C phases are observed, with variable temperature ranges. Interestingly, the nematic phases were found to exhibit cybotactic clusters with tilted SmC or orthogonal SmA structure (N_{CybC} or N_{CybA}) with wide temperature ranges. Finally, the isothermal photo switching because of *cis–trans* photoisomerization was investigated in solution as well as between different liquid crystal phases. This report could be of interest for optical information storage device applications.

1. Introduction

Due to their unique properties of combining order and mobility on a nanoscale level, liquid crystalline (LC) materials provide multiple functionalities [1]. They can respond to external fields such as light and electricity as well as to interaction with surfaces. Therefore, they are promising in many applications such as in liquid crystal displays (LCDs), semiconductors, photovoltaics, 5G antennae, smart windows, etc. [2–6]. Thermotropic LCs are classified according to their molecular shape into three main classes: calamitic (rod-like), discotic (disc-like), and bent-core (banana-shaped) LCs [7–11].

The LC behaviour could be tailored to specific applications by correct molecular design. There are several ways to control the type of LCs such as changing the length and type of the terminal flexible chains as well as the length of the aromatic backbone [12–15]. Another way to tailor LC properties is by changing the polar character of the organic molecule, which could be achieved by internal changes in the molecular structure. Therefore, different linking groups between the aromatic rings such as azo, ester or Schiff base have been used to design wide varieties of LCs [16–22]. The type of the linkage plays an important role in intermolecular interactions between the rigid cores in the condensed phase, which in turn affects the molecular organization in the LC phase. It could affect transition temperatures and the LC phase range. Also, inversion of the direction of the connecting group (e.g. -COO- and -OOC-) can lead to very different phase behaviour or even to the loss of the LC phase [23–26]. Because azobenzene-based LCs can undergo *trans–cis* photoisomerization, they are attractive candidates for technological applications including optical storage devices and nonlinear optics [27–30]. Therefore, different classes of azobenzene-based LCs with interesting properties were reported including rod-like, [31–33] discotic, [34,35] and banana-shaped LCs [10,36–39].

Modifying the overall polarity of a LC system is also possible by adding a lateral polar substituent to the rigid core at different positions or by attaching a polar group to the end of the flexible alkyl chain or at one end of the rigid core. These different strategies lead to changes in the LC behaviour as well as depression of melting points in case of lateral substitution. The lateral substituent decreases the length-to-breadth ratio in rod-like molecules and therefore changes the transition

* Corresponding author at: Institute of Chemistry, Martin Luther University Halle-Wittenberg, 06120 Halle, Germany.
E-mail addresses: mohamed.alaasar@chemie.uni-halle.de, malaasar@sci.cu.edu.eg (M. Alaasar).

https://doi.org/10.1016/j.molliq.2024.126174
Received 7 August 2024; Received in revised form 21 September 2024; Accepted 30 September 2024
Available online 2 October 2024

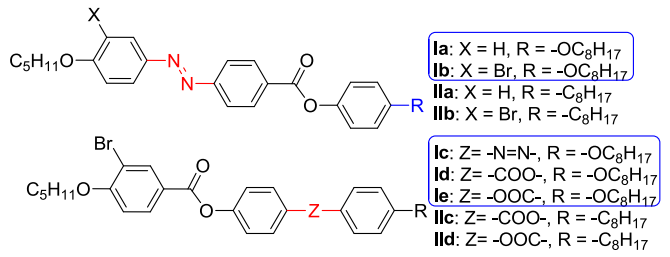

Fig. 1. Chemical structures of the synthesized materials **Ia–e** and **IIa–d**.

temperatures. The most commonly used lateral substituent is fluorine atom because of its unique combination of low polarizability and high polarity [40,41]. It has also played an important role in designing new LC materials exhibiting the interesting ferroelectric nematic phase [42–44]. On the other hand, less studies have been reported using bromine as a lateral substituent [45–50]. Bromine has more crystal volume of Immirzi (*cv* ~ 33 nm^3) [51] compared to fluorine (*cv* ~ 13 nm^3) [51], meaning that bromine results in more steric interaction and could lead to different phase behaviour.

The goal of this paper is to study the influence of aromatic core bromination on the liquid crystalline behaviour of rod-like compounds with different connecting groups. For this reason, we synthesised two series of new calamitic molecules with the same number of aromatic benzene rings and different connecting groups (**Ia–e** and **IIa–b**, Fig. 1). Therefore, a pentyloxy terminal chain was kept fixed at one end in both series, while the terminal chain attached to the other end was varied between an octyloxy chain (compounds **Ia–e**) or an octyl chain (compounds **IIa–d**). The effect of using different connecting groups such as azo or ester with different directions was systematically investigated. Inserting a lateral bromine substitution at ortho position with respect to the pentyloxy chain (**Ib–e** and **IIb–d**) was evaluated compared to the neat compounds without any lateral substitution (**Ia** and **IIa**). The materials were characterized for their phase behaviour by differential scanning calorimetry (DSC), polarized optical microscopy (POM) and X-ray diffraction (XRD). All compounds were found to be LCs with relatively wide ranges, which can be potentially used as smart dopants for the design of advanced multicomponent mixtures.

2. Experimental

2.1. Synthesis

The synthesis of the derivatives having the azo group close to the pentyloxy end (compounds **Ia, Ib, IIa** and **IIb**) was performed as shown in Scheme 1. To shift the position of the azo linkage to the other end (compounds **Ic–e** and **IIc–d**) another synthetic pathway was used as shown in Scheme 2.

As examples, the analytical data for two final compounds (**Ia** and **IIa**) are given below. The synthesis details and analytical data for all intermediates and the rest of the final materials are reported in the electronic supporting information (ESI).

Ia. Orange crystals, yield. 68.4 %. ^{1}H NMR (500 MHz, $CDCl_3$) δ 8.32 (d, J = 8.1 Hz, 2H, Ar-H), 7.97 (d, J = 8.4 Hz, 4H, Ar-H), 7.18–7.10 (m, 2H, Ar-H), 7.03 (d, J = 8.4 Hz, 2H, Ar-H), 6.98–6.91 (m, 2H, Ar-H), 4.07 (t, J = 6.6 Hz, 2H, Ar-O$\underline{CH_2}CH_2$), 3.97 (t, J = 6.6 Hz, 2H, Ar-O$\underline{CH_2}CH_2$), 1.90–1.75 (m, 4H, Ar-OCH$_2\underline{CH_2}$), 1.59–1.22 (m, 18H, 9×CH_2), 1.01–0.85 (m, 6H, 2×CH_3). ^{13}C NMR (126 MHz, $CDCl_3$) δ 165.10, 162.47, 156.97, 155.73, 146.87, 144.23, 131.14, 130.61, 125.30, 122.47, 122.34, 115.14, 114.84, 77.25, 76.99, 76.74, 68.46, 31.81, 29.35, 29.28, 29.23, 28.85, 28.15, 26.04, 22.65, 22.43, 14.08, 13.99.

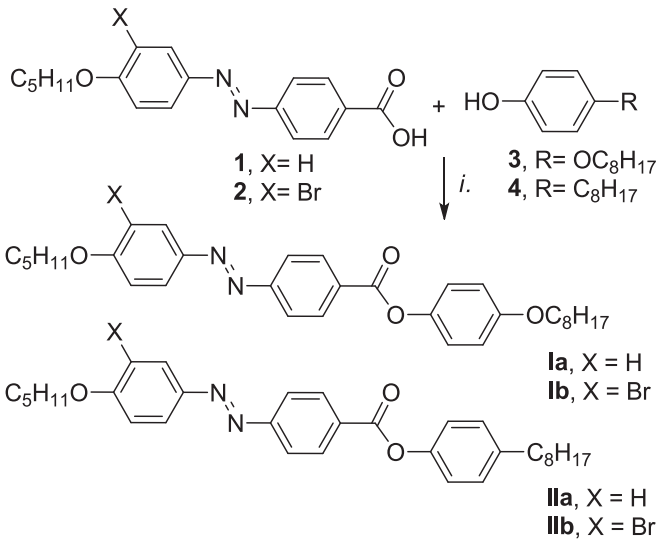

Scheme 1. Synthesis of the azobenzene-derived compounds **Ia, Ib, IIa** and **IIb**. Reagents and conditions: *i.* DCC, DMAP, dry dichloromethane, stirring at room temperature for 24 h.

HRMS: Calcd. for $C_{32}H_{40}N_2O_4$ $[M]^+$: 516.2982, found 516.2976.

IIa. Orange crystals, yield 62.1 %. ^{1}H NMR (500 MHz, $CDCl_3$) δ 8.33 (d, 2H, Ar-H), 7.97 (d, J = 8.7 Hz, 4H, Ar-H), 7.26–7.22 (m, 2H, Ar-H), 7.17–7.13 (m, 2H, Ar-H), 7.06–7.00 (m, 2H, Ar-H), 4.07 (t, J = 6.6 Hz, 2H, Ar-O$\underline{CH_2}CH_2$), 2.74–2.50 (m, 2H, Ar-$\underline{CH_2}CH_2$), 2.01–1.76 (m, 2H, Ar-OCH$_2\underline{CH_2}$), 1.69–1.18 (m, 18H, 9×CH_2), 1.03–0.75 (m, 6H, 2×CH_3). ^{13}C NMR (126 MHz, $CDCl_3$) δ 164.89, 162.46, 155.75, 148.81, 146.88, 140.65, 131.16, 130.63, 129.35, 125.29, 122.47, 121.27, 114.83, 77.25, 76.99, 76.74, 68.45, 35.40, 31.88, 31.47, 29.46, 29.29, 29.25, 28.85, 28.15, 22.66, 22.44, 14.09, 13.99. MS (ESI): HRMS: Calcd. for $C_{32}H_{40}N_2O_3$ $[M]^+$: 500.3033, found 500.3027.

3. Characterization

Analytical quality chemicals were obtained from commercial sources and used as obtained. The solvents were dried using standard methods when required. The purity and the chemical structures of all synthesised materials were confirmed by the spectral data. The structure characterization of the prepared materials is based on ^{1}H NMR and ^{13}C NMR (Varian Unity 400 spectrometers, in $CDCl_3$ solution, with tetramethylsilane as internal standard).

The mesophase behaviour and transition temperatures of the hydrogen-bonded complexes were measured using a Mettler FP-82 HT hot stage and control unit in conjunction with a Nikon Optiphot-2 polarizing microscope. The associated enthalpies were obtained from DSC-thermograms which were recorded on a Perkin-Elmer DSC-7, heating, and cooling rate: 10 K min^{-1}.

The photoisomerization studies in solution were conducted using Ocean Optics HR 2000+ spectrophotometer, and absorption spectra were recorded at room temperature. The solutions in chloroform were taken in a 1 cm quartz cuvette and covered to avoid the evaporation of the solvent. The solutions were irradiated with UV light of 1 mW/cm^2 using Bluepoint LED Eco Hönle at a wavelength of 365 nm. A heat filter is inserted between the sample and the source to avoid the influence of UV heat on the sample. The absorption spectra of the materials were investigated before and after UV illumination at varying time intervals.

The *trans–cis-trans* photoisomerization in the LC phase was

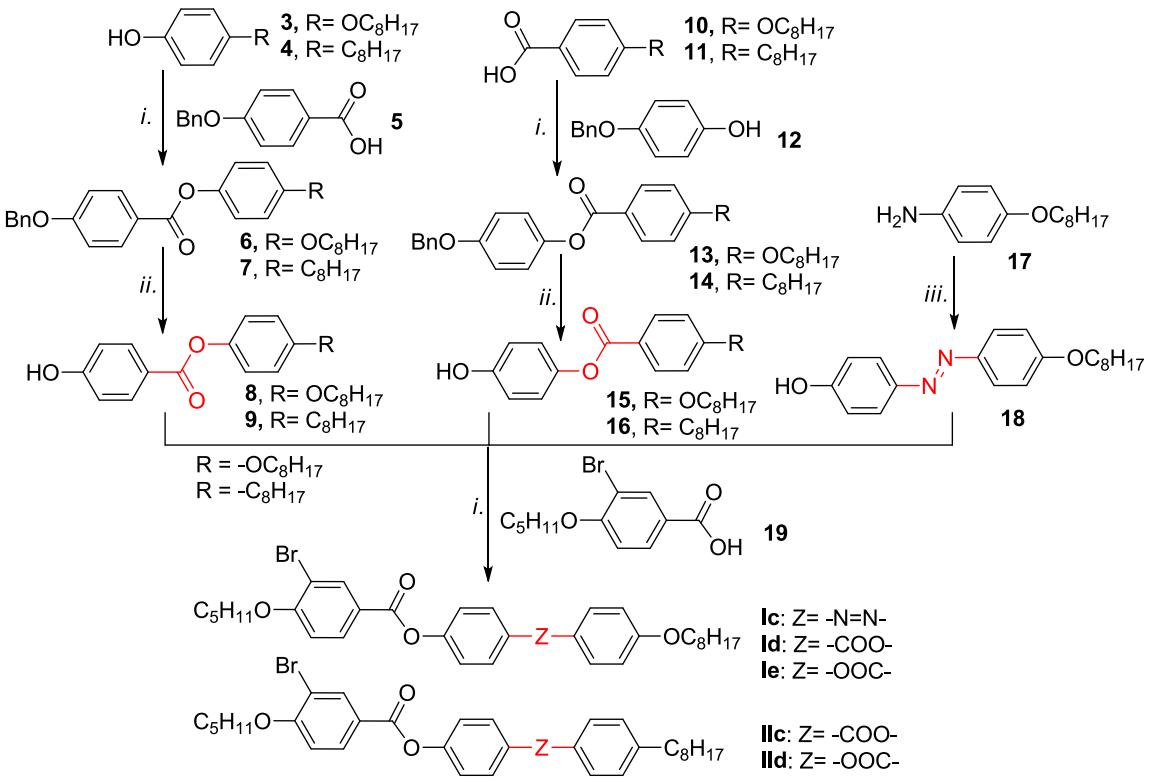

Scheme 2. Synthesis of compounds **Ic–e** and **IIc–d**. Reagents and conditions: *i.* DCC, DMAP, dry dichloromethane, stirring 24 h; *ii.* Pd/C-10 %, dry THF, stirring at room temperature 24 h; *iii.* 1. $NaNO_2$, Conc. HCl, 2. Phenol, NaOH.

Table 1
Phase transition temperatures (T/°C), mesophase types, and transition enthalpies [ΔH (kJ/mol)] of compounds **Ia–e**.[a]

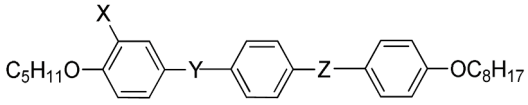

Cpd.	X	Y	Z	Transition Temperatures (*T*/°C [ΔH (kJ/mol)])
Ia	H	-N=N-	-COO-	**H:** Cr 107 [37.3] SmC_s 129 [0.3] N 220 [1.3] Iso **C:** Iso 218 [−1.3] N 127 [−0.3] SmC_s 84 [−35.8] Cr
Ib	Br	-N=N-	-COO-	**H:** Cr 104 [32.0] N 176 [0.7] Iso **C:** Iso 174 [−0.8] N 102 [−1.1] SmC_s 77 [−46.6] Cr
Ic	Br	-COO-	-N=N-	**H:** Cr 116 [28.1] N 180 [1.3] Iso **C:** Iso 176 [−1.3] N 97 [-1.7] SmC_s 88 [−20.6] Cr
Id	Br	-COO-	-COO-	**H:** Cr 114 [37.0] N 171 [1.2] Iso **C:** Iso 167 [−1.0] N 109 [−1.6] SmC_s 84 [−25.5] Cr
Ie	Br	-COO-	-OOC-	**H:** Cr 115 [28.9] N 176 [1.6] Iso **C:** Iso 172 [−1.5] N 113 [−4.5] SmC_s 75 [−22.1] Cr

[a] Peak temperature as determined from 2nd heating (**H**) and 2nd cooling (**C**) DSC scans with rate 10 K min^{-1}; abbreviations: Cr = crystalline solid; SmC_s = synclinic smectic C phase; N = nematic phase; Cr = crystalline solid; Iso = isotropic liquid.

Table 2
Phase transition temperatures (T/°C), mesophase types, and transition enthalpies [ΔH (kJ/mol)] of compounds **IIa–d**.[a]

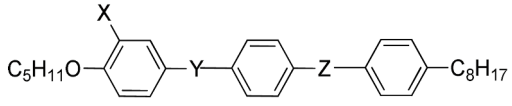

Cpd.	X	Y	Z	
IIa	H	-N=N-	-COO-	**H:** Cr 88 [46.4] SmA 148 [<0.1][b] N 201 [0.8] Iso **C:** Iso 199 [−0.8] N 146 [<0.1][b] SmA 65 [−33.2] Cr
IIb	Br	-N=N-	-COO-	**H:** Cr 60 [22.1] SmC_s 70 [0.6] N 152 [0.6] Iso **C:** Iso 149 [−0.6] N 67 [−0.7] SmC_s
IIc	Br	-COO-	-COO-	**H:** Cr 102 [19.1] N 152 [0.7] Iso **C:** Iso 148 [−0.8] N 100 [−3.1] SmC_s 70 [−9.4] Cr
IId	Br	-COO-	-OOC-	**H:** Cr 109 [36.0] N 146 [1.2] Iso **C:** Iso 144 [−1.1] N 88 [−1.3] SmC_s 80 [−30.5] Cr

[a] Peak temperature as determined from 2nd heating (**H**) and 2nd cooling (**C**) DSC scans with rate 10 K min^{-1}; for abbreviations see Table 1.
[b] This transition could not be detected by DSC and determined only under POM.

performed using Bluepoint LED Eco Hönle at a wavelength of 365 nm.

X-ray investigations were carried out with an Incoatec (Geesthacht, Germany) IμS microfocus source with a monochromator for CuKα radiation (λ = 0.154 nm), calibration with the powder pattern of Pb $(NO3)_2$. A droplet of the sample was placed on a glass plate on a Linkam hot stage HFS-X350-GI (rate: 1 K/min). Exposure time was 5 min; the sample-detector distance was 9.00 cm for WAXS and 26.80 cm for SAXS. The diffraction patterns were recorded with a Vantec 500 area detector (Bruker AXS, Karlsruhe) and transformed into 1D plots using GADDS software.

4. Results and discussion

4.1. Mesomorphic properties

The phase transition temperatures and phase types of the new

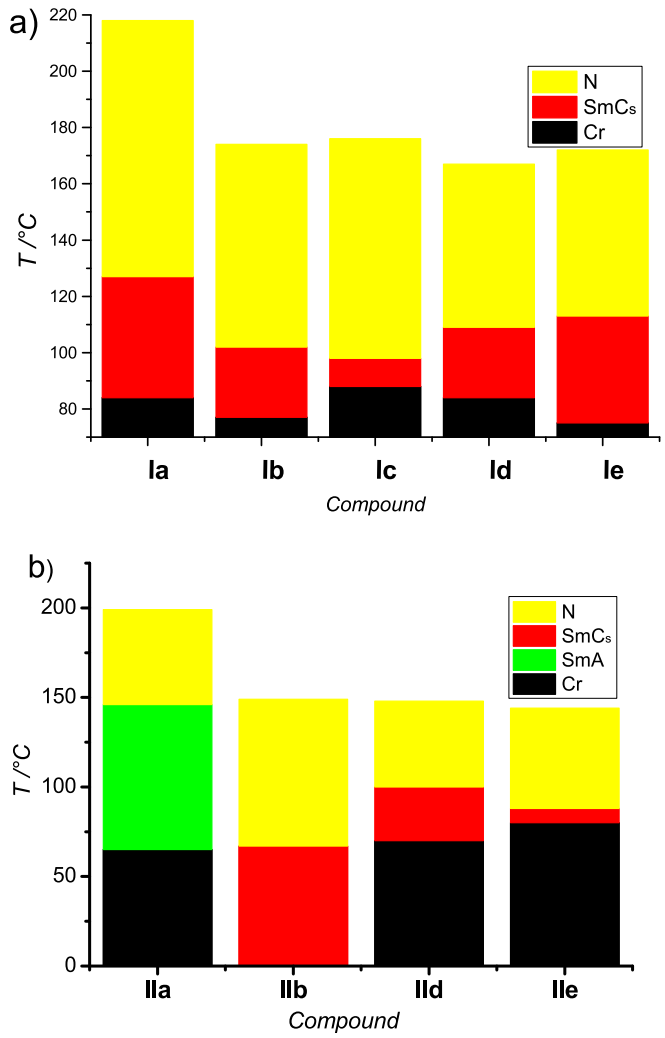

Fig. 2. Phase diagrams of (a) compounds **Ia–e** and (b) compounds **IIa–d** on cooling.

materials were revealed based on textural observations made under POM and on DSC measurements. The recorded transition temperatures and type of mesophases exhibited by **Ia–e** and **IIa–d** are summarized in Table 1 and Table 2, respectively. The data are also represented graphically on Fig. 2a, b.

In addition to the parent materials without any lateral substitution used in this study (**Ia** and **IIa**), the introduction of lateral bromine group, changing the position of the azo linkage, the direction of the ester group and changing the type of terminal flexible chain at one end allow systematic studies of the mesophase behaviour exhibited by the synthesized materials.

4.2. Non-substituted derivatives

As can be seen from Tables 1, 2 and Fig. 2 the neat compounds (**Ia** and **IIa**) without any lateral substitution exhibit two different types of LC phases depending on the type of the terminal chain (see Fig. 3 for DSC). Both materials have the same connecting groups, and they differ only in the terminal chain attached at one end, where **Ia** has an octyloxy chain and **IIa** has an octyl chain without the oxygen atom linking the flexible chain to aromatic ring. This small change in the molecular structure leads to a dramatic change in the phase behaviour.

Therefore, two LC phases are observed for both materials as indicated in Tables 1 and 2. It also has a great effect on the transition temperatures, where **Ia** has a melting temperature of ~107 °C which is

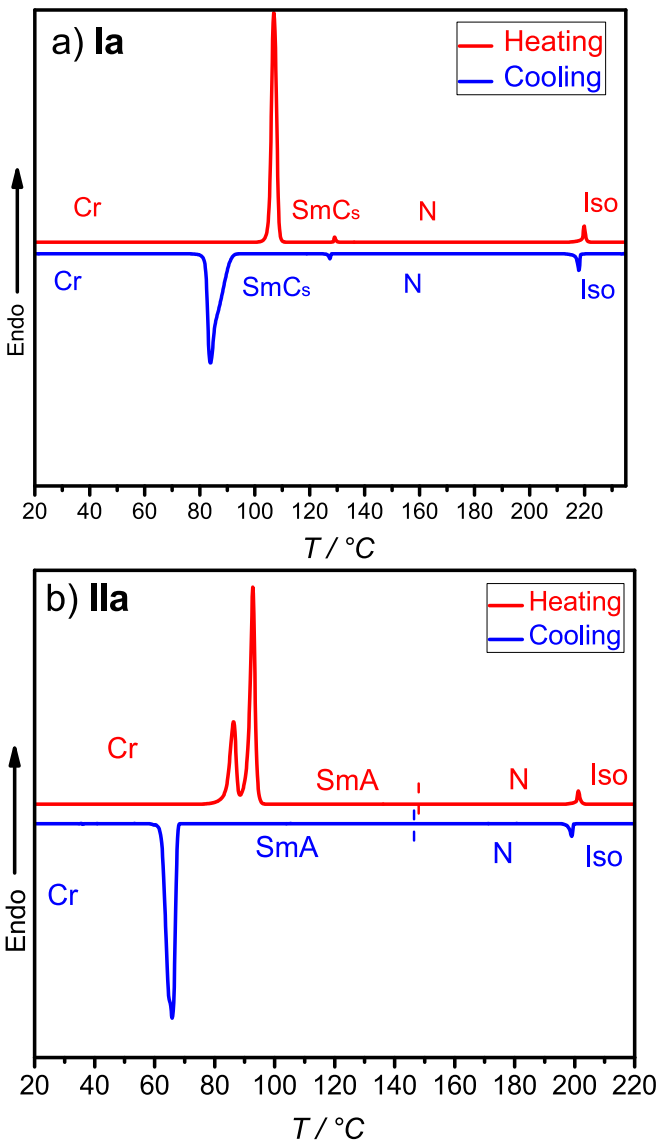

Fig. 3. DSC traces of (a) **Ia** and (b) **IIa** with heating and cooling rates 10 K min^{-1}.

higher than that of **IIa** (~88 °C). However, both materials have the same LC range ~113 K. On cooling **Ia** in normal homeotropic cell from the isotropic liquid phase under POM a transition to a Schlieren texture is observed (see for example Fig. 4a). This Schlieren texture is typically observed for nematic (N) phase and therefore this LC phase is assigned as N phase. On further cooling the N phase a transition to another LC phase occurs at ~127 °C, which is also measurable on DSC cooling cycle with a transition enthalpy of 0.3 kJ/mol. indicating a first order phase transition (Table 1). This phase is characterized by high birefringence and four brush disclinations, which is a characteristic feature of the synclinic smectic C phase (SmC_s) [12]. Therefore, this lower temperature phase is assigned as SmC_s phase, which crystallizes on further cooling of **Ia** at ~84 °C. Using a 10 μm ITO planar cell a dark texture is observed in the whole range of the N phase (Fig. 4c) and broken fan-shaped texture with the dark extinctions inclined with the direction of the polarizers confirming the presence of SmC_s phase.

Replacing the octyloxy chain in **Ia** by octyl chain in **IIa** reduces the melting and clearing temperatures, retains the higher temperature N phase and more interesting removes the lower temperature SmC_s observed for **Ia**. As indicated from the POM investigations another LC phase is observed on cooling the N phase of **IIa** under POM, which is

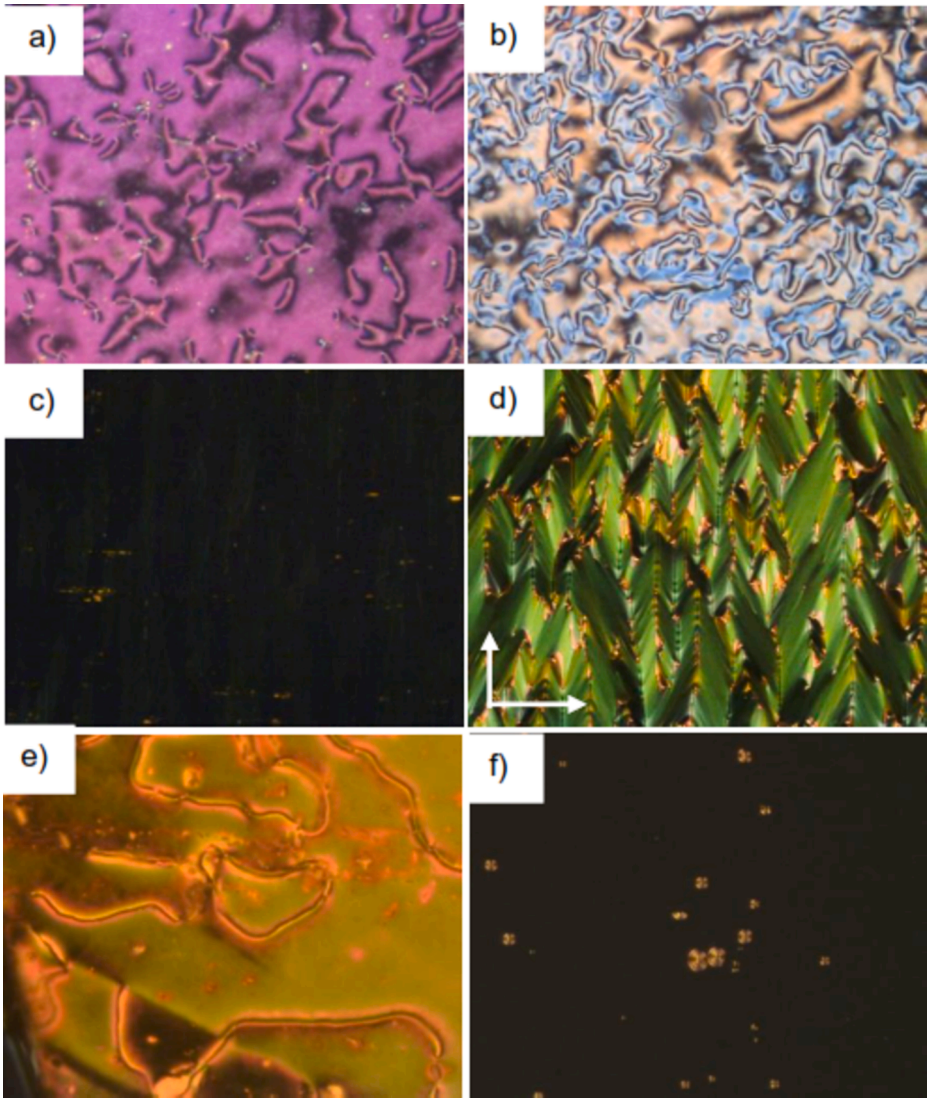

Fig. 4. Optical textures observed on cooling for: **Ie** in a homeotropic cell (a) N phase at 160 °C, (b) SmC_s phase at 90 °C. **IIb** in a 10 μm ITO planar cell: (c) in N phase at 140 °C and (d) in SmC_s phase at 55 °C. **IIa** in a homeotropic cell (e) N phase at 180 °C and (f) SmA at 135 °C. The scale bar is 100 μm in all textures. The textures of the SmC_s phase shown in d) remains till room temperature without observation of crystallization (see Fig. S19 in the SI for the DSC traces of **IIb**).

characterized by its homeotropic appearance (Fig. 4f). On applying shearing stress on this lower temperature LC a birefringent texture is observed, which immediately relaxes back to the homeotropic texture indicating the presence of orthogonal smectic A (SmA) phase. The transition from N to SmA is not detectable by DSC and can be only observed by POM, meaning that this transition is a second order phase transition. The SmA phase is found to be enantiotropic phase observed on heating and cooling over a relatively wide temperature ranges ~60 and 81 K, respectively. This phase was further proved by XRD (see Section 4.2).

4.3. Effect of aromatic core bromination

To investigate the effect of aromatic core bromination in comparison to the neat compounds (**Ia** and **IIa**) we have synthesized compounds **Ib** and **IIb**. As can be seen from Tables 1, 2 and Fig. 2a, b, the melting temperatures as well as clearing points in both cases are reduced compared to **Ia** and **IIa**. This could be attributed to the steric effect resulting from using the large bromine atom at the terminal ring in both types of compounds, which leads to this change of transition temperatures without destroying the liquid crystalline nature of the resulting materials. Therefore, in case of **Ib** the SmC_s phase is observed as a metastable phase instead of an enantiotropic one as that recorded for **Ia**. On the other hand, the SmA phase observed for **IIa** is replaced by a SmC_s one because of lateral bromine substitution in case of **IIb**. This SmC_s phase is enantiotropic, and its formation is accompanied by detectable transition enthalpies both on heating and cooling DSC cycles, meaning a first order phase transition. More interesting the SmC_s phase remains on cooling **IIb** till ambient temperature without crystallization (Fig. S19). These observations indicate that the effect of core bromination is more pronounced in case of series **II**, where it results in replacing SmA by SmC_s phase and successfully leads to the formation of a room temperature LC phase, which could be of interest for applications.

Exchanging the position of the azo linkage in case of **Ib** with the ester unit leads to compound **Ic**. This retains the same phase sequence and types observed for **Ib** but slightly increases the melting, clearing and crystallization temperatures, which results in a smaller range of SmC_s phase ~9 K for **Ic**. The difference in the phase behaviour between **Ib** and **Ic** could be understood based on the increased dipole moment in case of **Ic** compared to **Ib** because of connecting the ester group directly to the brominated benzene ring.

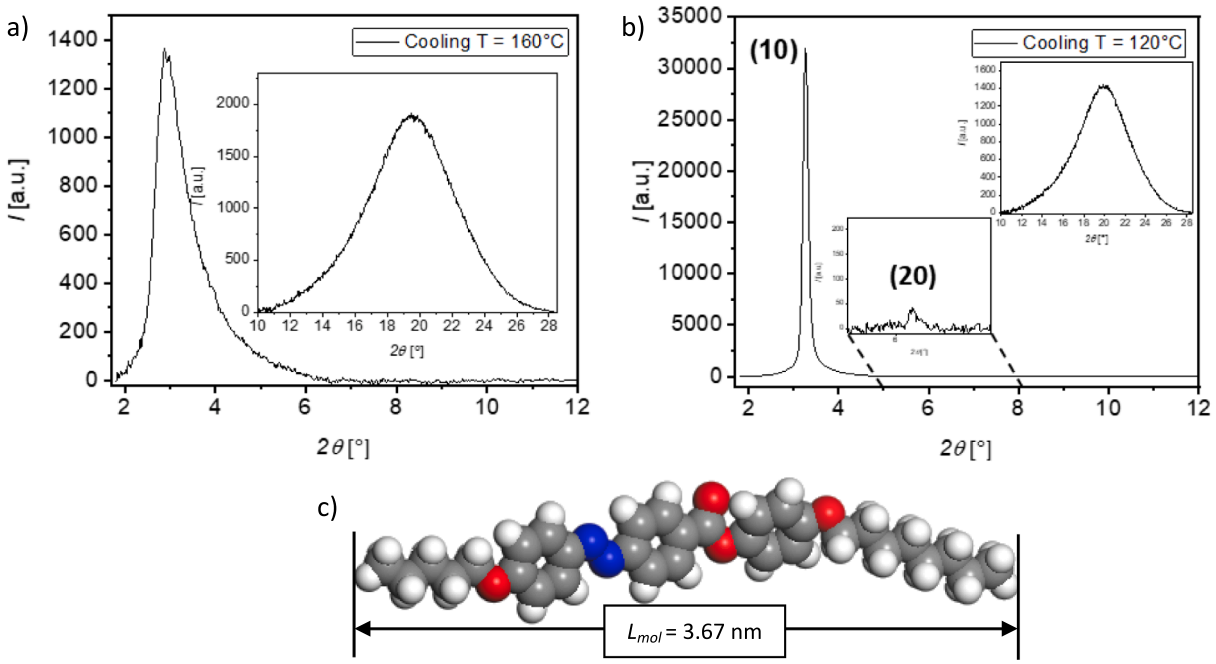

Fig. 5. Plot of the integrated scattered intensity as a function of 2θ in the small-angle region (SAXS) for **Ia** on cooling: (a) the N phase at $T = 160$ °C, (b) the SmC_s phase at $T = 120$ °C, (c) CPK model of compound **Ia** showing the calculated molecular length (L_{mol}). The insets in (a) and (b) show the WAXS region in both phases.

4.4. *Effect of replacing the azo linkage with an ester unit*

To investigate the effect of replacing the azo linkage with an ester unit we synthesized compounds **Id**, **Ie** from the first group of materials and compounds **IIc** and **IId** related to the second type. Comparing compounds **Ib** and **Id** reveals that replacing the azo linkage with an ester group retains the same phase sequence and types but increases the melting and crystallization temperatures, which in turn results in narrower LC range for **Id**. The same trend of increasing melting and crystallization temperatures also applied for **IIb** and **IIc**. However, because of the large increasing of the melting temperature of **IIc** ~ 102 °C compared to **IIb** ~ 60 °C the enantiotropic SmC_s displayed by **IIb** appears as a monotropic one in case of **IIc**, which crystallizes at ~70 °C on cooling.

This could be explained by the increased dipole moment resulting from using the ester group, which in turn increases the core-core interactions leading to such dramatic change of the transition temperatures. Therefore, using azo linkage is more efficient than ester one toward mesomorphism in these materials.

Inverting the direction of one ester group in **Id** and **IIc** results in compounds **Ie** and **IId**, respectively. This modification does not lead to a dramatic change in the phase behaviour as it retains the same phase sequence on heating and cooling for all four materials with only a slight change in all transition temperatures.

4.5. *XRD investigations*

To confirm the LC phase types XRD experiments were carried out for all materials. All measurements were performed using a surface-aligned sample. Alignment was achieved by slow cooling of a small drop of the sample from the isotropic liquid state on a glass substrate.

On cooling **Ia** from the isotropic liquid and in the range of the higher temperature LC phase (at T ~ 160 °C) a diffuse wide-angle scattering (WAXS) reflex at $d = 0.45$ nm is observed indicating a mesophase with no fixed positions of the molecules, typically observed for the LC state (Fig. 5a). The SAXS pattern recorded at T ~ 160 °C shows one small

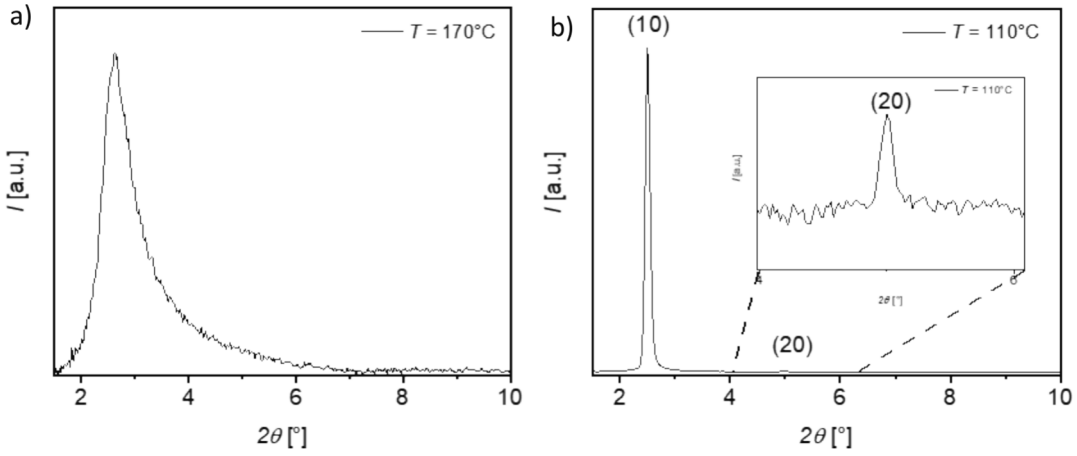

Fig. 6. Plot of the integrated scattered intensity as a function of 2θ in the small-angle region (SAXS) for **IIa**: (a) the N phase at $T = 170$ °C and (b) the SmA phase at $T = 110$ °C.

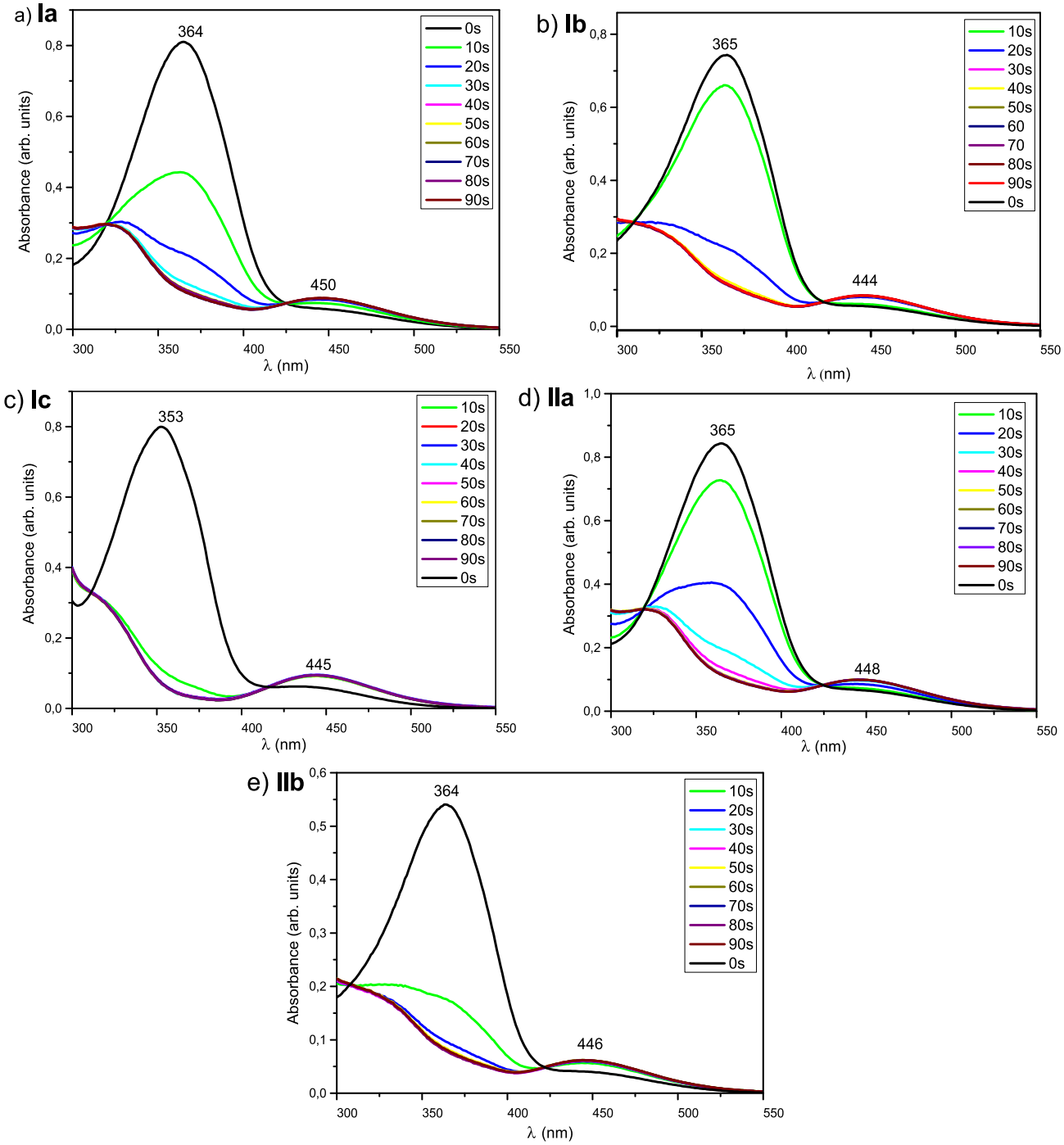

Fig. 7. Spectral changes observed under UV light irradiation for: (a) **Ia**, (b) **Ib**, (c) **Ic**, (d) **IIa** and (e) **IIb**.

angle scattering peak at $2\theta \sim 3.0°$. The peak is relatively sharp, and its intensity increased with decreasing temperature in the N phase and become very sharp at the transition to the lower temperature Sm phase (Fig. 5b). The appearance of a sharp peak in the N phase is unusual behaviour as usually only a broad halo scattering is observed for conventional nematic of rodlike LCs [52]. This single peak corresponds to d value of ~2.98 nm, which is lower the molecular length of the compound calculated with Materials Studio for all-trans conformation of the alkyl chains $L_{mol} = 3.67$ nm (Fig. 5c). The presence of this sharp peak and this calculated d-value suggest the presence of cybotactic clusters of SmC-like structure (CybC) in the nematic phase of **Ia** and therefore the nematic phase could be assigned as N_{CybC}. This was also supported by the appearance of a streak-like Schlieren texture (Fig. S26a) in the N phase under POM, which is typically observed for such phase [53–55]. The N_{CybC} phase is common for bent-core LCs [56–60] but only few examples were reported for calamitic LCs [53,61–64] and it was recently reported for polycatenar molecules [65].

On further cooling the recorded SAXS and in the temperature range of the lower temperature Sm phase at $T \sim 120$ °C the small angle scattering turns into a sharper Bragg reflex with $d \sim 2.70$ nm and its second-order reflex, indicating a layer-like structure (Fig. 5b). The estimated d-value is smaller than that observed in the N_{CybC} phase and less than the molecular ($L_{mol} = 3.67$ nm). This can be explained by forming a layer-like structure with tilted molecules in a smectic C phase. Assuming a SmC structure in line with the optical textures (Fig. S26b) and the XRD pattern with a tilt angle β of ~35° calculated according to $\cos\beta = d/L_{mol}$.

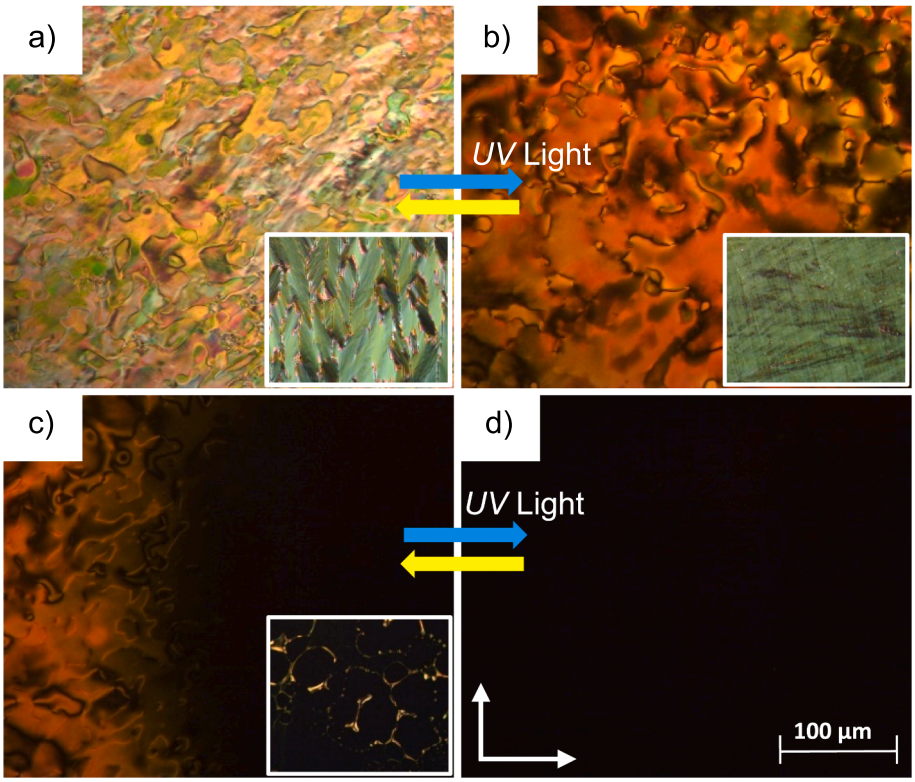

Fig. 8. Reversible isothermal photo-off–on switching between the different LC phases of compound **IIb**. (a,b) Between SmC_s and N phases at 65 °C, (c) at the transition from the N to the isotropic phase at 140 °C and (d) in the isotropic phase. The insets show the textures in the corresponding LC phases using 10 μm ITO planar cell.

We have also investigated compound **IIa** having the same connecting groups as **Ia** but with terminal octyl chain instead of the alkoxy chain with XRD (Fig. 6). Like **Ia** a sharp peak could be detected in the SAXS region in the N phase, which also become sharper with decreasing temperature being very sharp in the Sm phase region. This again indicates the presence of cybotactic clusters in the N phase which fused to layer structure in the Sm phase. The *d* value calculated in the N phase is $d \sim 3.32$ nm, which is lower the molecular length $L_{mol} = 3.56$ nm (Fig. S49). The *d*-value in the lower temperature Sm phase is ~ 3.52 nm, which is close to $L_{mol} = 3.56$ nm meaning the presence of SmA phase.

This in line with observation of a homeotropic texture for this LC phase under POM (Fig. 4f) and confirming the presence of a SmA phase. More interesting this means that the cybotactic clusters in the upper temperature nematic phase are of SmA type, leading to phase assignment of N_{CybA} [60]. This phase is relatively rare even for bent-core LCs and is of particular interest from the application point of view as it is expected to exhibit faster switching time than that of uniaxial nematics [56]. To the best of our knowledge compound **IIa** represents the third case of N_{CybA} phase in rod-like LCs [53,61].

Investigating the remaining members of series **I** as well as those of series **II** i.e. the brominated materials **Ib–e** and **IIb–IId** with XRD revealed similar data to their parent neat compounds **Ia** and **IIa** (see Section 3 in the SI). However, the peak observed in the N phase for brominated compounds is not as sharp as that observed for unsubstituted materials **Ia** and **IIa**, meaning that the N phase still has cybotactic clusters, but it seems to be smaller in size. The reason for this could be explained based on the steric effect of the bulky bromine group which results in partial distortion of the clusters in the nematic phase.

4.6. Photo switching

4.6.1. Photoisomerization in solution

The photoisomerization properties of the azobenzene-based materials **Ia–c** and **IIa–b** with/without bromine substitution and different orientation of the ester group were investigated. All compounds were dissolved in chloroform and their solutions were measured with UV–Vis spectrometry before and after UV illumination with time intervals of 10 s (Fig. 7).

Before UV light irradiation all compounds exhibit a prominent absorption band between 364 and 365 nm except compound **Ic** (~353 nm). This absorption band corresponds to the π–π* transition indicating the presence of the most stable *trans* isomer for all materials. After UV light illumination this band starts to decrease and another weak absorption band around 445–450 nm starts to appear, which is due to the *n*–π* transition corresponding to the less stable *cis* isomer. These observations confirm the *trans–cis* photoisomerization of the azo group under UV illumination. All materials show complete *trans–cis* conversion within ~30 s, except compound **Ic**. For this compound a complete photoisomerization is observed within ~10 s (Fig. 7c) which is the fastest time among all materials. Also, the wavelength of the *trans* isomer of **Ic** appears at lower wavelength value ~353 nm compared to all other derivatives ~365 nm. Both observations indicate that indeed the position and orientation of the ester linkage group play an important role as **Ic** is the only investigated compound having the COO unit close to the pentyloxy terminal chain. This results in higher conjugation and more dipole moment of **Ic** compared to other analogues giving rise to such different photoisomerization behaviour. Storing the solutions overnight in the dark after UV irradiation and investigating them again leads typical spectra observed at zero seconds before UV irradiation in all cases, meaning complete isothermal back relaxation from *cis* to *trans* isomer.

It is also interesting that all materials exhibit photoconversion efficiency (PCE) of more than 85 % after UV illumination, making them excellent candidates for optical storage device applications [37,66]. The PCE i.e. the extent of photoisomerization, was calculated according to Eq. (1), where $A(t_0)$ is the initial absorbance (before UV irradiation) and

$A(t_\infty)$ is the final absorbance (after UV irradiation).

$$PCE = \frac{A(t_0) - A(t_\infty)}{A(t_0)} \times 100 \quad (1)$$

4.6.2. Photo switching between LC phases

To study the possibility of isothermal photo switching between the different types of LC phases exhibited by the azobenzene-based synthesized materials we have selected compound **IIb** for such investigations. This compound displays enantiotropic N and SmC_s phases. Under isothermal UV light irradiation (365 nm) in the lower temperature SmC_s phase at $T = 65$ °C a transition to the N phase takes place in less than three seconds (Fig. 8a, b). The insets in Fig. 8a, b show the textures in the corresponding LC phases using a 10 μm ITO planar cell, showing the transition from the broken-fan shaped textures of the SmC_s phase to the characteristic marble texture of the N phase. On switching off the light source the texture relaxes back immediately to the initial texture of the SmC phase. The same observations were also recorded on performing the same investigations in the N phase, where a rapid transition to the isotropic liquid phase is recorded (Fig. 8c, d). This transition is also fast and reversible as that between SmC_s and N phases under light irradiation. These observations confirm the possibility of isothermal photo switching between the different LC phases because of *trans–cis* photoisomerization of the azobenzene moiety under light irradiation. This phenomenon could be of interest for optical information storage device applications [37,66].

5. Summary and conclusions

In summary, we have reported the synthesis and investigations of new light-responsive rod-like liquid crystalline materials aiming to study the effect of aromatic core bromination as well as using different linking groups on the phase behaviour in a systematic manner. We represented two new series of such materials having three benzene rings connected using different linking groups either azo or ester units with different directions. In both series a pentyloxy chain was used at one end, where an octyl or an octyloxy chain was attached to the other end. In both series, a lateral bromine substituent was inserted at ortho position with respect to the pentyloxy chain. Additional modifications were performed by replacing the azo linkage by an ester one or by inverting the direction of the ester group. Depending on the absence or presence of the lateral substituent, linking units and the terminal chain three different types of LC phases were observed including the SmC_s, SmA or N phase. The formation and stabilities of the LC phases depend strongly on the mentioned factors. Interestingly, all nematic phases found to exhibit cybotactic clusters of the tilted SmC type or the non-tilted version i.e. the SmA as proved from the XRD investigations. The observation of N_{CybC} or N_{CbyA} is not common for rod-like LCs and is well known for BCLCs. We have also investigated the reported azobenzene-based materials for their isothermal *cis–trans* photoisomerization in solution as well as in bulk state. All materials exhibit fast photoisomerization in solution, which depends on the type of the linking groups. Also, a fast and a reversible photo switching between different LC states was recorded under POM. The photo responsive materials reported herein could be used as smart dopants for multicomponent mixtures with potential applications for nonlinear optics or optical information storage devices.

CRediT authorship contribution statement

Mohamed Alaasar: Writing – review & editing, Writing – original draft, Supervision, Project administration, Investigation, Funding acquisition, Conceptualization. **Tejal Nirgude:** Methodology, Investigation. **Christian Anders:** Writing – review & editing, Investigation.

Declaration of competing interest

The authors declare that they have no known competing financial interests or personal relationships that could have appeared to influence the work reported in this paper.

Data availability

No data was used for the research described in the article.

Acknowledgements

This work was supported by the German Research Foundation (DFG) for the financial support (AL2378/1-2, 424355983, RTG 2670, 436494874).

Appendix A. Supplementary material

Supplementary data to this article can be found online at https://doi.org/10.1016/j.molliq.2024.126174.

References

[1] S.T. Lagerwall, Ferroelectric and Antiferroelectric Liquid Crystals, Wiley-VCH, Weinheim, 1999.
[2] M. Bremer, P. Kirsch, M. Klasen-Memmer, K. Tarumim, The TV in your pocket: development of liquid-crystal materials for the new millennium, Angew. Chem. Int. Ed. 52 (2013) 8880.
[3] R. Jakoby, A. Gaebler, C. Weickhmann, Microwave liquid crystal enabling technology for electronically steerable antennas in SATCOM and 5G millimeter-wave systems, Crystal 10 (2020) 514.
[4] T. Kato, J. Uchida, T. Ichikawa, T. Sakamoto, Functional liquid crystals towards the next generation of materials, Angew. Chem. Int. Ed. 57 (2018) 4355.
[5] M. Alaasar, Y. Cao, T. Neumann, T. Tan, F. Liu, M. Giese, Halogen substituted bithiophene-based polycatenars with tunable fluorescence, Mater. Adv. (2024), https://doi.org/10.1039/D4MA00771A.
[6] A. Murad, M. Alaasar, A.F. Darweesh, A. Eremin, Effect of fullerene doping on electronic and photovoltaic properties of the cubic bicontinuous phase, Mater. Adv. 5 (2024) 6205.
[7] Non-conventional liquid crystals, in: J.W. Goodby, P.J. Collings, H. Gleeson, P. Raynes, T. Kato, C. Tschierske (Eds.), Handbook of Liquid Crystals, second edition, vol. 5, Wiley-VCH, Weinheim, 2014.
[8] M. Gupta, A. Krishna, S. Sony, S. Dhingra, A. Shah, D.P. Singh, First examples of room-temperature discotic nematic liquid crystals exhibiting ambipolar charge carrier mobilities, Chem. Commun. 59 (2023) 10652.
[9] C. Tschierske, Development of structural complexity by liquid-crystal self-assembly, Angew. Chem. Int. Ed. 52 (2013) 8828.
[10] M. Alaasar, Azobenzene-containing bent-core liquid crystals: an overview, Liq. Cryst. 43 (2016) 2208.
[11] R.A. Reddy, C. Tschierske, Bent-core liquid crystals: polar order, superstructural chirality and spontaneous desymmetrisation in soft matter systems, J. Mater. Chem. 16 (2006) 907.
[12] M. Alaasar, S. Poppe, Hockey-Stick polycatenars: network formation and transition from one dimensional to three-dimensional liquid crystalline phases, J. Mol. Liq. 351 (2022) 118613.
[13] O.A. Alhaddad, M.S. Khushaim, S.M. Gomha, H.A. Ahmed, M.M. Naoum, Mesophase behavior of four ring ester/azomethine/ester liquid crystals in pure and mixed states, Liq. Cryst. 49 (2022) 1395.
[14] T. Zong, R. Mandle, I. Saez, S. Cowlingand, J. Goodby, Rods to discs in the study of mesomorphism in discotic liquid crystals, Liq. Cryst. 45 (2018) 2274.
[15] Y. Arakawa, Y. Ishida, Y. Sasaki, S. Sasaki, M. Tokitac, H. Tsuji, Alkylthio-based asymmetric liquid crystals: unravelling the substituent effects and intercalated cybotactic nematic and smectic phases, Mater. Adv. 3 (2022) 3218.
[16] M. Pfletscher, C. Wölper, J.S. Gutmann, M. Mezger, M. Giese, A modular approach towards functional supramolecular aggregates–subtle structural differences inducing liquid crystallinity, Chem. Commun. 52 (2016) 8549.
[17] S. Aya, P. Salamon, D.A. Paterson, J.M.D. Storey, C.T. Imrie, F. Araoka, A. Jakli, A. Buka, Fast-and-giant photorheological effect in a liquid crystal dimer, Adv. Mater. Interf. 6 (2019) 1802032.
[18] A. Eremin, H. Nadasi, P. Hirankittiwong, J. Kiang-Ia, N. Chattham, O. Haba, K. Yonetake, H. Takezoe, Azodendrimers as a photoactive interface for liquid crystals, Liq. Cryst. 45 (2018) 2121.
[19] M. Pfletscher, M. Mezger, M. Giese, On the impact of linking groups inhydrogen-bonded liquid crystals – a case study, Soft Matter 14 (2018) 621.
[20] S. Chen, Y. Li, Z. Guo, T. Ma, Y. Tao, Y. Duan, Y. Yang, X. Cheng, Fluorescent columnar liquid crystals based on BTD hexacatenars with salicylaldimine and benzaldimine core: self-assembly and multifunctional properties, J. Mol. Liq. 403 (2024) 124803.

[21] K. Katariya, R. Soni, K.J. Nakum, D. Patel, S. Nada, M. Hagar, New symmetric/unsymmetrical self-assembling salicylaldimine-chalcones: synthesis, photophysical study and DFT approach, J. Mol. Str. 1295 (2024) 136610.
[22] M.-M. Iftime, V. Cozan, A. Airinei, C. Varganici, G. Ailiesei, D. Timpu, I. Sava, Asymmetric azomethine amines with azobenzene moieties – liquid crystalline and optical properties, Liq. Cryst. 46 (2019) 1584.
[23] M. Duan, T. Tasaka, H. Okamoto, V.F. Petrov, S. Takenaka, Liquid crystalline properties of dissymmetric molecules IV. The substituent effect on thermal properties of nematic and smectic A phases in three aromatic ring systems with ester linkages, Liq. Cryst. 27 (2000) 1195.
[24] M. Alaasar, M. Prehm, M. Poppe, M. Nagaraj, J.K. Vij, C. Tschierske, Development of polar order and tilt in lamellar liquid crystalline phases of a bent-core mesogen, Soft Matter 10 (2014) 5003.
[25] M. Poppe, M. Alaasar, A. Lehman, S. Poppe, M.-G. Tamba, M. Kurachkina, A. Eremin, M. Nagaraj, J.K. Vij, X. Cai, F. Liu, C. Tschierske, Controlling the formation of heliconical smectic phases by molecular design of achiral bent-core molecules, J. Mater. Chem. C 8 (2020) 3316.
[26] A. Lehmann, M. Alaasar, M. Poppe, S. Poppe, M. Prehm, M. Nagaraj, S. P. Sreenilayam, Y.P. Panarin, J.K. Vij, C. Tschierske, Stereochemical rules govern the soft self-assembly of achiral compounds: understanding the heliconical liquid-crystalline phases of bent-core mesogens, Chem. Eur. J. 26 (2019) 4714.
[27] H. Yu, T. Ikeda, Photocontrollable liquid-crystalline actuators, Adv. Mater. 19 (2011) 2149.
[28] O.S. Bushuyev, A. Tomberg, T. Friščić, C.J. Barrett, Shaping crystals with light: crystal-to-crystal isomerization and photomechanical effect in fluorinated azobenzenes, J. Am. Chem. Soc. 135 (2013) 12556.
[29] H.K. Bisoyi, Q. Li, Light-driven liquid crystalline materials: from photo-induced phase transitions and property modulations to applications, Chem. Rev. 116 (2016) 15089.
[30] R.S. Zola, H.K. Bisoyi, H. Wang, A.M. Urbas, T.J. Bunning, Q. Li, Dynamic control of light direction enabled by stimuli-responsive liquid crystal gratings, Adv. Mater. 31 (2018) 1806172.
[31] M. Alaasar, M. Prehm, Y. Cao, F. Liu, C. Tschierske, Spontaneous mirror-symmetry breaking in isotropic liquid phases of photoisomerizable achiral molecules, Angew. Chem. Int. Ed. 128 (2016) 320.
[32] M. Alaasar, S. Poppe, Q. Dong, F. Liu, C. Tschierske, Isothermal chirality switching in liquid-crystalline azobenzene compounds with non-polarized light, Angew. Chem. Int. Ed. 56 (2017) 10801.
[33] S. Bin, W.S. Yam, G. Hegde, Photoresponsive behavior of hydrophilic/hydrophobic-based novel azobenzene mesogens: synthesis, characterization and their application in optical storage devices, RSC Adv. 9 (2019) 40588.
[34] M. Sperner, N. Tober, H. Detert, Tristriazolotriazines with azobenzene arms - acidochromic dyes and discotic liquid crystals, Eur. J. Org. Chem. 2019 (2019) 4688.
[35] G.S. dos Santosab, E. Westphal, Photoisomerizable azobenzene star-shaped liquidcrystals: bypassing the absence of hydrogenbonding, New J. Chem. 46 (2022) 7334.
[36] M. Alaasar, X. Cai, Y. Cao, F. Liu, Transition from lamellar to nanostructure mesophases in azobenzene-based hockey-stick polycatenars, New J. Chem. 46 (2022) 15871.
[37] B.S. Ranjitha, D.S. Kumari, A. Shetty, G. Shanker, M. Alaasar, R. Pashameah, G. Hegde, Impact of terminal group on azobenzene liquid crystal dimers for photo-responsive optical storage devices, J. Mol. Liq. 383 (2023) 121985.
[38] Y. Arakawa, K. Komatsu, Y. Ishida, H. Tsuji, Thioether-linked azobenzene-based liquid crystal dimers exhibiting the twist-bend nematic phase over a wide temperature range, Liq. Cryst. 48 (2021) 641.
[39] M. Alaasar, M. Prehm, S. Belau, N. Sebastián, M. Kurachkina, A. Eremin, C. Chen, F. Liu, C. Tschierske, Polar order, mirror symmetry breaking, and photoswitching of chirality and polarity in functional bent-core mesogens, Chem. Eur. J. 25 (2019) 6362.
[40] M. Hird, Fluorinated liquid crystals – properties and applications, Chem. Soc. Rev. 36 (2007) 2070.
[41] C. Tschierske, Fluorinated liquid crystals: design of soft nanostructures and increased complexity of self-assembly by perfluorinated segments, Top. Curr. Chem. 318 (2012) 318.
[42] C.J. Gibb, J. Hobbs, D.I. Nikolova, T. Raistrick, S.R. Berrow, A. Mertelj, N. Osterman, N. Sebastián, H.F. Gleeson, R.J. Mandle, Spontaneous symmetry breaking in polar fluids, Nat. Commun. 15 (2024) 5845.
[43] S. Brown, E. Cruickshank, J.M.D. Storey, C.T. Imrie, D. Pociecha, M. Majewska, A. Makal, E. Gorecka, Multiple polar and non-polar nematic phases, Chem. Phys. Chem. 22 (2021) 2506.
[44] J. Karcz, J. Herman, N. Rychlowicz, P. Kula, E. Gorecka, J. Szydlowska, P. W. Majewsi, D. Pochiecha, Spontaneous chiral symmetry breaking in polar fluid–heliconical ferroelectric nematic phase, Sci. 384 (2024) 1096.
[45] N. Podoliak, V. Novotná, M. Kašpar, V. Hamplová, M. Glogarová, D. Pociecha, Anomalous phase sequence in new chiral liquid crystalline materials, Liq. Cryst. 41 (2014) 176.
[46] N. Podoliak, V. Hamplová, M. Kašpar, V. Novotná, M. Glogarová, D. Pociecha, E. Gorecka, High tilted smectogens with bromine-substituted molecular core, Liq. Cryst. 40 (2013) 321.
[47] M. Kašpar, A. Bubnov, V. Hamplová, Z. Málková, S. Pirkl, M. Glogarová, Effect of lateral substitution by fluorine and bromine atoms in ferroelectric liquid crystalline materials containing a 2-alkoxypropanoate unit, Liq. Cryst. 34 (2007) 1185.
[48] P. Fernandes, P. Barois, E. Grelet, F. Nallet, J.W. Goodby, M. Hird, J.-S. Micha, Extension of the resonant scattering technique to liquid crystals without resonant element, Eur. Phys. J. E 20 (2006) 81.
[49] P. Cluzeau, P. Gisse, V. Ravaine, A.-M. Levelut, P. Barois, C.C. Huang, F. Rieutord, H.T. Nguyen, Resonant X-ray diffraction study of a new brominated chiral SmC_A^* liquid crystal, Ferro. 244 (2000) 1.
[50] Y. Takanishi, I. Nishiyama, J. Yamamoto, Y. Ohtsuka, A. Iida, Remarkable effect of a lateral substituent on the molecular ordering of chiral liquid crystal phases: a novel bromo-containing dichiralcompound showing SmC* variants, J. Mater. Chem. 21 (2011) 4465.
[51] A. Immirzi, B. Perini, Prediction of density in organic crystals, Acta Cryst. A33 (1977) 216.
[52] B.S. Ranjitha, M. Alaasar, G. Shanker, Super-cooled chiral fluorescent liquid crystal dimers with reduced symmetry, J. Mol. Str. 1305 (2024) 137626.
[53] Y. Arakawa, Y. Ishida, Y. Sasaki, S. Sasaki, M. Tokita, H. Tsuji, Alkylthio-based asymmetric liquid crystals: unravelling the substituent effects and intercalated cybotactic nematic and smectic phases, Mater. Adv. 3 (2022) 3218.
[54] C. Tschierske, D.J. Photinos, Biaxial nematic phases, J. Mater. Chem. 20 (2010) 4263.
[55] S.J. Picken, T.J. Dingemans, L.A. Madsen, O. Francescangeli, E.T. Samulski, Uniaxial to biaxial nematic phase transition in a bent-core thermotropic liquid crystal by polarising microscopy, Liq. Cryst. 39 (2012) 19.
[56] C. Keith, A. Lehmann, U. Baumeister, M. Prehm, C. Tschierske, Nematic phases of bent-core mesogens, Soft Matter 6 (2010) 1704.
[57] H. Ocak, B.B. Eran, S. Nuray, A. Özkonstanyan, S. Poppe, C. Tschierske, Extraordinary magnetic field effects on the LC phases of homochiral and racemic 4-cyanoresorcinol-based diamagnetic bent-core mesogens, J. Mater. Chem. C 9 (2021) 1895.
[58] M. Alaasar, M. Prehm, C. Tschierske, New azobenzene containing bent-core liquid crystals based on disubstituted resorcinol, Liq. Cryst. 41 (2014) 126.
[59] M. Alaasar, S. Poppe, C. Kerzig, C. Klopp, A. Eremin, C. Tschierske, Cluster phases of 4-cyanoresorcinol derived hockey-stick liquid crystals, J. Mater. Chem. C 5 (2017) 8454.
[60] A. Nasir, M. Rahman, Cybotactic nematic liquid crystal – an overview, Liq. Cryst. 51 (2024) 503.
[61] W. Nishiya, Y. Takanishi, J. Yamamoto, A. Yoshizawa, Molecular design for a cybotactic nematic phase, J. Mater. Chem. C 2 (2014) 3677.
[62] Y. Uchida, T. Akita, K. Hanada, D. Kiyohara, N. Nishiyama, Molecular clustering behaviour in the cybotactic nematic phase of a spin-labelled liquid crystal, J. Mater. Chem. C 10 (2022) 6621.
[63] Y. Kimoto, A. Nishizawa, Y. Takanishi, A. Yoshizawa, J. Yamamoto, Anomaly of pretransitional behavior at the nematic–smectic-a phase transition of amphiphilic liquid crystals with a hydrophilic group, J. Phys. Chem. B 117 (2013) 6290.
[64] Y. Arakawa, Y. Sasaki, K. Igawa, H. Tsuji, Hydrogen bonding liquid crystalline benzoic acids with alkylthio groups: phase transition behavior and insights into the cybotactic nematic phase, New J. Chem. 41 (2017) 6514.
[65] M. Alaasar, S. Poppe, Cybotactic nematic phases with wide ranges in photoresponsive polycatenars, Liq. Cryst. 47 (2020) 939.
[66] D.S. Kumari, A. Shetty, B.S. Ranjitha, M. Vandana, G. Shanker, M. Alaasar, G. Hegde, Spectroscopic investigation on shuttlecock-shaped liquid crystalline trimers: mesomorphic behaviour and its application in optical storage devices, Heliyon 10 (2024) e37455.